

PROGRESS ON COMPUTATION OF BOILING FLOW IN FUEL ASSEMBLIES WITH NEPTUNE_CFD

C. Baudry, N. Mérioux, J. Laviéville, S. Mimouni and M. Guingo

Electricité de France, R&D Division
6 Quai Watier, 78401 Chatou, France
cyril.baudry@edf.fr

ABSTRACT

In previous works, we have evaluated Computational Fluid Dynamics results obtained with NEPTUNE_CFD against single-phase liquid water tests equipped with a mixing vane and against two-phase boiling cases (DEBORA-tube and ASU-annular channel tests [1]). In the present work, a geometry closer to actual fuel assemblies is considered. It consists of a rectangular test section including a 5x5 rod bundle, four meters long, equipped with seven mixing vane spacer grids, two non mixing vane spacers and eight single spacers. This fuel assembly design is taken from the specifications of the PWR Subchannel and Bundle Tests (PSBT) benchmark. This benchmark is an international project endorsed by the OECD/NEA and supported by US NRC and METI (Japan), in which a large experimental database of void-fraction measurements has been made available [2].

This computation is performed with the released version of NEPTUNE_CFD 2.3 based on a consistent set of models: a RANS approach with a Reynolds-Stress Model is used for the turbulence modeling of the continuous phase; whereas the drag force from Ishii [3], the added mass from Zuber [4], the lift force from Tomiyama [5] and a turbulent dispersion force are chosen for the dispersed phase.

The study of this 5x5 rod bundle case is a further step towards a physically reliable local CFD modeling, confirming the adequacy of this approach for the industrial application. It contributes to build an expertise in two-phase boiling flows and DNB phenomenology inside fuel assemblies.

KEYWORDS

Two-Phase Flow, CFD, Boiling Flow, Industrial Application, Fuel bundle

1. INTRODUCTION

High-thermal performance PWR (Pressurized Water Reactor) spacer grids require low pressure loss, high wall heat transfer coefficient and high critical heat flux (CHF) properties. A further detailed understanding of the main physical phenomena (wall boiling, entrainment of bubbles in the wakes, recondensation) is needed and can be approached by numerical simulation.

In Shin et al [6], a Critical Heat Flux (CHF) experiment on the effect of the angle and of the position of mixing vanes was performed in a 2x2 rod bundle. The authors show that the mixing vanes increase the value of the CHF and the result is correlated to the magnitude of the swirl generated by the mixing vanes. If the angle of the mixing vanes is relatively small, the magnitude of the swirling flow is smaller because the rotating force created by the mixing vanes is weak. On the opposite, if it is relatively large, the mixing vanes play the role of flow obstacle and therefore may decrease the CHF. Therefore, it is important that the turbulence modeling deals correctly with rotation effects.

There have been several studies on flow mixing and heat transfer enhancement caused by a mixing-vane spacer grid in a rod bundle. Ikeda et al. [7] studied an assembly consisting of a 5x5 heater rod bundle and eight specific mixing vane spacers. For Ikeda et al., it might be insufficient to apply a standard $k-\epsilon$ model to swirl-mixing flow in narrow-channel flow conditions that includes non-isotropic effects. Moreover, In et al. [8] performed a series of CFD single phase flow simulations to analyze the heat transfer enhancement in a fully heated rod bundle with mixing-vane spacers. For future work, In et al. recommend that a refined Computational Fluid Dynamic (CFD) model be developed to include details of the grid structure and a higher-order turbulence model be employed to improve the accuracy of such simulations. Lee et al. [9] simulated the flow field and heat transfer in a single phase flow for a 17x17 rod bundle with eight spans of mixing vanes. The FLUENT commercial code was employed and a Reynolds Stress Transport Model (RSTM) was used for turbulence. According to the authors, RSTM is well adapted to this flow configuration. Liu et al. [10] compare several turbulence models and experimental data for lateral and axial distributions for Nusselt number. For Liu et al., the SST $k-\omega$ turbulence model is better suited due to an adapted near-wall treatment.

Additional two-phase effects like accumulation of bubbles in the center of a sub-channel or vapor pockets on the rods should be taken into account to improve the simulation of flow close to DNB (departure from nucleate boiling). Indeed, single-phase simulations remain insufficient and boiling flows simulations are required. In Krepper et al. [11], the authors described CFD approaches to subcooled boiling and investigated their capability to contribute to fuel assembly design. A large part of their work was dedicated to the modeling of boiling flows and to forces acting on the bubbles. The authors noted that the size of bubbles in the bulk is correlated to the local subcooling which is an important parameter (see [1]).

The NEPTUNE_CFD code [12] was validated with a RSTM approach on a single-phase flow with mixing vanes and on more academic cases of air-water adiabatic bubbly flows in a pipe [13]. Then, the RSTM approach on boiling flows was validated [14] on AGATE-mixing experiment [15] and DEBORA-mixing experiment [17]. Mimouni et al. [14] has studied the impact of a detailed description of the bubble size on the boiling flow and the sensitivity to the angles of the vanes in a 2x2 rod bundle.

Based on what is discussed above, the objective of the present work is twofold:

- to gain insight into detailed two-phase 3D phenomena occurring in a PWR fuel assembly in boiling conditions, especially concerning the effect of spacers grids and mixing vanes ;
- to explore the practical issues implied when addressing real industrial geometries and meshes for industrial fuel assemblies.

To this aim, we carried out simulations of a 5x5 bundle configuration corresponding to the OECD/NRC PWR Subchannel and Bundle Tests (PSBT) benchmark, an international project endorsed by the OECD/NEA and supported by US NRC and METI (Japan). In this project, a large experimental database of void-fraction measurements performed under PWR thermal-hydraulic conditions in different geometric configurations (different types of isolated subchannels or rod bundles) has been made available to the participants. One of the purposes of this benchmark is to provide experimental data that can be used for the validation of numerical models of void-fraction distribution over a wide range of operating conditions, and for the development of novel approaches.

We consider two geometries:

- a full geometry with 2 non-mixing vanes, 7 mixing vanes and 8 simple spacers 3.8 meters long,
- a partial geometry with 1 non-mixing vane, 1 mixing vane and 1 simple spacer, 0.8 meters long (last section of the assembly).

The CFD simulations of boiling flows in these large fuel sub-assemblies constitute a pioneering work raising many challenging issues, on physical modeling, on meshing methodology and on all Information Technology (IT) questions implied by handling very large data sets at the different stages of the process.

The standard set of parameters of the code for boiling bubbly two-phase flow is applied, with in particular the use of a second-order (Reynolds stress) turbulence model.

1.1 Main features of the NEPTUNE_CFD code

The NEPTUNE_CFD code, which is based on an Eulerian two-fluid model, is developed within the framework of the NEPTUNE project, financially supported by EDF (Electricité de France), CEA (Commissariat à l'Énergie Atomique et aux Energies Alternatives), IRSN (Institut de Radioprotection et de Sûreté Nucléaire) and AREVA-NP. NEPTUNE_CFD is mainly focused on Nuclear Reactor Safety applications involving two-phase flows, like two-phase Pressurized Thermal Shock and Departure from Nucleate Boiling. It inherits the I/O and High Performance Computing (HPC) capabilities of the EDF open-source CFD software Code_Saturne [16] used as a pre-requisite library, can be coupled with the SYRTHES solid-conduction code for conjugate heat transfer simulation and can be used as a module of the SALOME plate-form.

The NEPTUNE_CFD code follows the classical multifield one-pressure formulation [18], and the spatial discretization is based upon a full unstructured finite-volume approach with a collocated arrangement of all-variables. The numerical algorithm used is a semi-implicit, pressure-based method where the system of equations is solved in two major fractional steps: first, a prediction of the velocities based on the momentum equations; then, the coupling between phase fraction, pressure and energy through mass and energy equations and a simplified form of momentum equations [19].

1.2 Experimental configuration

The test facility of the rod bundle test represents a partial section and the full length of the 17x17 type PWR fuel assembly. Rods are arranged in 5x5 square array. The effective heated length is 3658 mm where the void measuring sections are located at 2216 mm (Lower), 2669 mm (Middle) and 3177 mm (Upper) from the bottom of the heated length.

The void fraction is measured by using the chromo-tomography (CT) technique, which also gives the local distribution of the time-averaged void-fraction at the measuring section. Four parameters are taken into account in the PSBT benchmark:

- outlet pressure,
- mass flux,
- inlet temperature,
- heating power.

The value of the controlling parameters of the runs and the cross-section averaged void-fraction measurements are summarized in Table 1. The input parameters for the run simulated in the present work correspond to the test conditions referenced 5.2442 [1].

For these simulations, we use a uniform axial power shape, with 25 heated rods. The radial power distribution is described in Table 2.

Table 1 Main flow parameters of the computations.

Parameter	Values
Outlet pressure (bar)	147.07
Inlet temperature (°C)	263.0
Inlet mass flow rate (kg/m ² /s)	1386.11
Wall heat flux (MW)	2.000

Table 2 Radial power distribution.

0.85	0.85	0.85	0.85	0.85
0.85	1	1	1	0.85
0.85	1	1	1	0.85
0.85	1	1	1	0.85
0.85	0.85	0.85	0.85	0.85

2. CAD AND MESHING STRATEGY

Geometry is described in Table 3.

Table 3 Geometry of rod bundle assembly.

Item	data
Rods array	5×5
Number of heated rods	25
Heated rod outer diameter (mm)	9.50
Heated rods pitch (mm)	12.60
Axial heated length (mm)	3658
Number of MV spacers	7
Number of NMV spacers	2
Number of simple spacers	8
MV spacer location (mm)	471, 925, 1378, 1832, 2285, 2739, 3247
NMV spacer location (mm)	2.5, 3755
Simple spacer location (mm)	237, 698, 1151, 1605, 2059, 2512, 2993, 3501

For this complex geometry, only blueprints were available. Therefore, we used the software SALOME 7.2 [14] to first make the CAD (Computer-Aided Design) geometry, and then, for the meshing stage. In the CAD and mesh construction process, we considered four different blocks:

- simple spacer (SP),
- non-mixing vane (NMV),
- mixing vane (MV),
- 2D pattern with different extrusion length.

In Figure 1, a partial view of the CAD can be found. Due to the complexity of the problem, we opted for a conformal joining between the blocks. For the SP, NMV and MV parts, we use CAD to make a surface mesh with the SALOME built-in BLSURF tool. Then, we used this one and the 2D pattern (Figure 2) to build tetrahedron 3D meshing with the TETMESH-GHS3D algorithm. Regular parts between vanes and spacers are made of hexahedra.

Finally, we obtained four meshes:

- simple spacer : 4.8 million cells,
- non-mixing vane : 10.9 million cells,
- mixing vane : 19.2 million cells,

The complete mesh of the full bundles then counts 256 million cells.

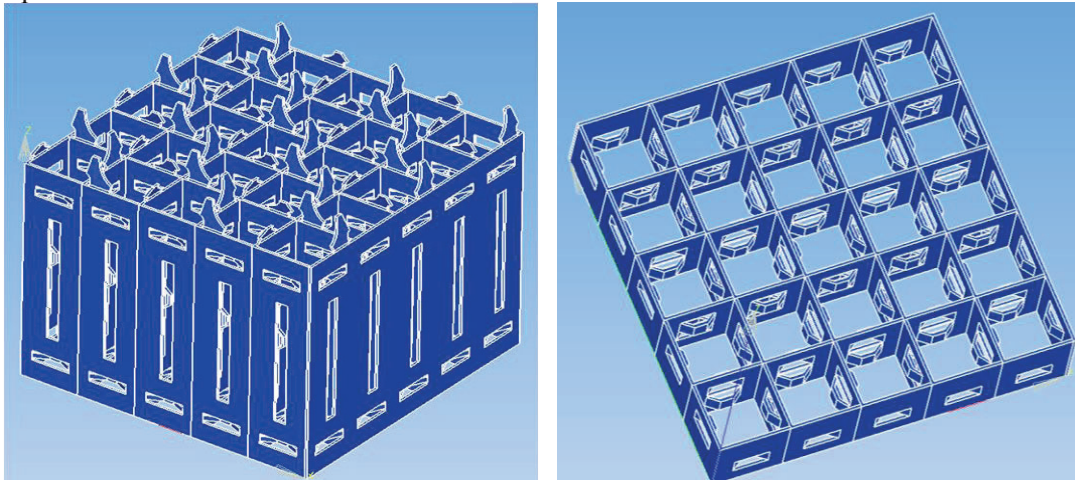


Figure 1. Part of the CAD model.

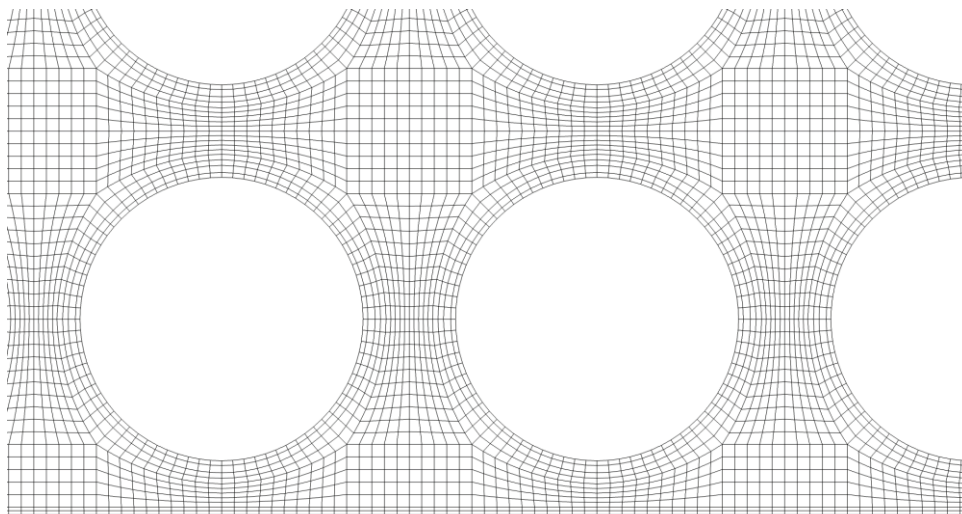


Figure 2. Mesh pattern to join meshes.

Then, we evaluated quality of the meshes, following the Best Practice Guidelines. We summarize quality information for the mixing vane (MV) and the simple spacer (SS) in Table 4. Particularly, we observed one crucial quality indicator for NEPTUNE_CFD: the maximum non-orthogonality angle is less than 69° and less than 0.01% of cells have non-orthogonality angle lying between 60° and this maximum value. Test on mesh sensitivity were performed for PSBT sub-channel but for the 5x5 geometry, this is more complicated due to simulation time.

Table 4 quality criteria: histogram of the boundary faces non-orthogonality angle (in degrees).

	histogram of the interior faces weighting coefficient	histogram of the interior faces non-orthogonality angle (in degrees)	histogram of the boundary faces non-orthogonality angle (in degrees)
MV			
SS			

3. PHYSICAL MODELING

The turbulence of the liquid phase is modeled using a second-order, RANS model (Reynolds Stress Model) [14] including bubble-induced turbulence effects, whereas a turbulent dispersion model is applied on the gas phase [21]. The interfacial transfer of momentum is considered as the sum of different contributions: the drag force (modeled by using the correlation developed by Ishii [1]), the added mass force (by using the expression of Zuber [4]) and the formulation of the lift force proposed by Tomiyama [5].

No flow-regime map is used here, as the flow is regarded as bubbly. No parameter-tuning with respect to the experimental results has been attempted.

At the heating wall, the heat transfer model is an extension of the approach of Kurul et al. [22] (often referred to as the RPI model) consisting in splitting the heat flux into three terms: one heating the liquid phase in contact with the wall, one responsible for the bubble generation and the last one arising from the arrival of liquid water at the wall, caused by bubble departure (the so-called “quenching” flux). When the void fraction in the boundary cells is sufficiently high, a fourth flux is introduced to take into account the convective heat transfer transmitted to the vapor.

The bubble detachment diameter is given by the correlation from Unal et al. [23]. The Unal’s correlation is valid for subcooled liquid but has been extended to saturated liquid. In order to take into account the influence of bubbles in the near-wall area, a modified logarithmic law of the wall was introduced [24].

For calculations, the bubble-size distribution has been studied by performing simulations using the interfacial area model of Ruyer & Seiler [25], which has been validated in PWR conditions in vertical duct geometry. The interfacial area concentration a_i is directly connected to the local void fraction α and the Sauter mean diameter d_{32} the following relation $a_i = \frac{6 \alpha}{d_{32}}$. The Ruyer-Seiler model assumes a quadratic form

for the bubble-diameter distribution. In this model, coalescence and break-up phenomena are taken into account.

In general, models were selected according to the validation of NEPTUNE_CFD 1.0.8 for bubbly flow [1].

The NEA/CSNI Best Practice Guidelines [24] were followed as much as possible, especially in the mesh generation process by keeping acceptable quality for the grids and also by assessing the numerical convergence.

4. RESULTS

4.1. Computational strategy

An initial single phase computation on full bundle has been performed. The mean fluid velocity is around 6 m/s, we estimate to have to compute a minimum of 2 physical seconds to ensure convergence (3 times the transit time across the domain) for the full bundle.

At the beginning of the simulation, we impose a heat flux equal to zero to initialize the computational domain. Between 10^{-4} and 10^{-3} s of simulation time, the power increases from zero to the nominal value.

To ensure a fast convergence, we use the newly-developed “steady” algorithm [25] in the first phase of the simulation. After convergence is obtained with this method, we swap to adaptive (transient) numerical algorithm to rigorously control convergence.

We perform the computations on an x86-64 computer architecture with a Linux operating system. The computations for the full bundle runs on 1980 cores. For a two-phase bubbly simulation, we use a memory of around 700 Megabytes for 100.000 cells on memory.

To control convergence, we plot:

- The mass balance and energy balance evolution for each fuel rods and outlet for each phase,
- The pressure, temperatures, velocities, bubble diameter and volume fractions on 6 probes per plane (Figure 3), 10 planes for the full bundle (Figure 4).

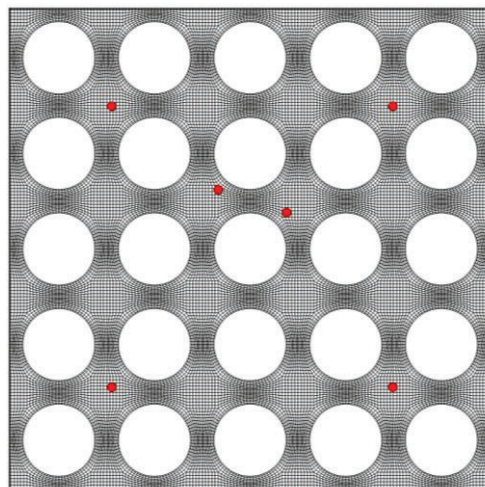


Figure 3. Probes locations in a plane.

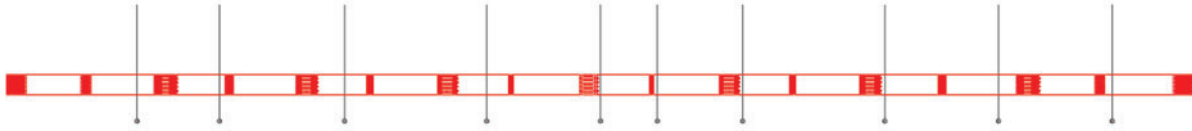


Figure 4. Planes localization for probes along the fuel assemble.

Finally, the typical time step is around $5 \cdot 10^{-5}$ s. The numerical convergence is reached after 3 seconds of simulation time and we simulate 3.4 s at the end (Figure 1). Between 0 and 2 seconds, complex physical phenomena can be observed: vapor production, condensation, dynamics phenomena due to spacers, etc... At the end, we have equilibrium between all phenomena.

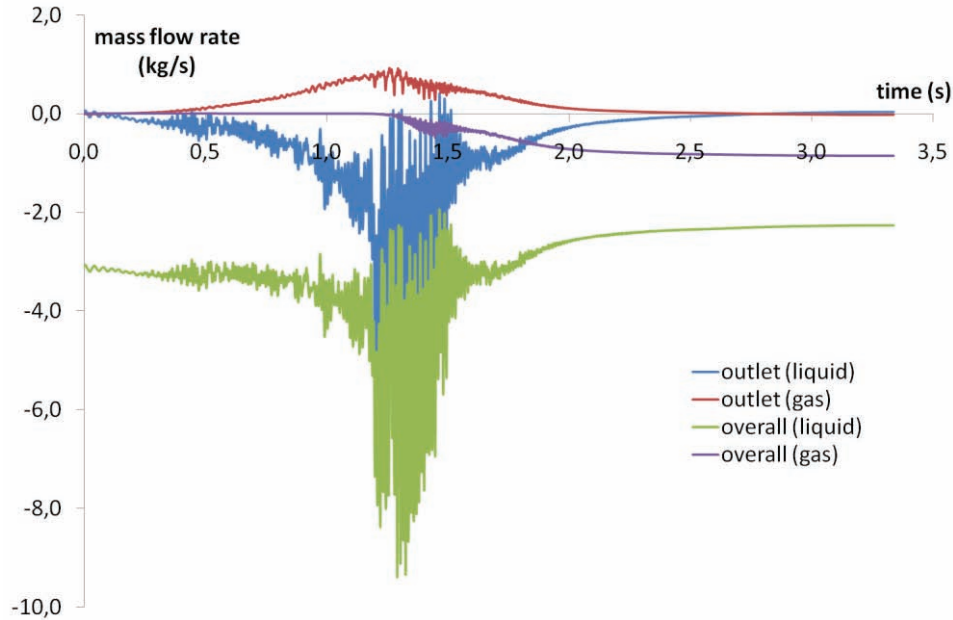


Figure 5. Mass flow rate evolution.

4.2. Results analysis

The aim of the present section is to analyze the dynamics of the flow and to provide indicators of the quality of the results. We compute the hydraulic diameter D_h from the central sub channel, with formula $D_h = \frac{4 \cdot A}{P}$, where A is the cross sectional area and P is the wetted perimeter of the cross-section. The hydraulic diameter D_h is around 11.78 mm. Mean values are computed for the central sub-channel.

1. Pressure drop

We compute the mean pressure per section for the central subchannel for the simulation and we plot relative mean pressure ($P - P_{\text{output}}$). The influence of spacers can be observed on Figure 6. Then, we evaluate the pressure drop due to spacers. For simple spacers, the pressure drop is between $1.6 \cdot 10^3$ Pa and $4.7 \cdot 10^3$ Pa. For mixing vanes, the pressure drop is between $3.2 \cdot 10^3$ Pa and $8.3 \cdot 10^3$ Pa. The pressure drop increases with void fraction, in good agreement with the momentum conservation .

The only data available for code-to-data comparison is the pressure drop over the heated section for bundle B7 in [2]. However, a code-to-code comparison has been performed for pressure drop over heated length

of the typical central sub-channel and for the bundle. For the run5.2442, the pressure drop obtained by the benchmark participants was around $6 \cdot 10^4$ Pa. Here, we obtain a pressure drop around 10^5 Pa for the bundle.

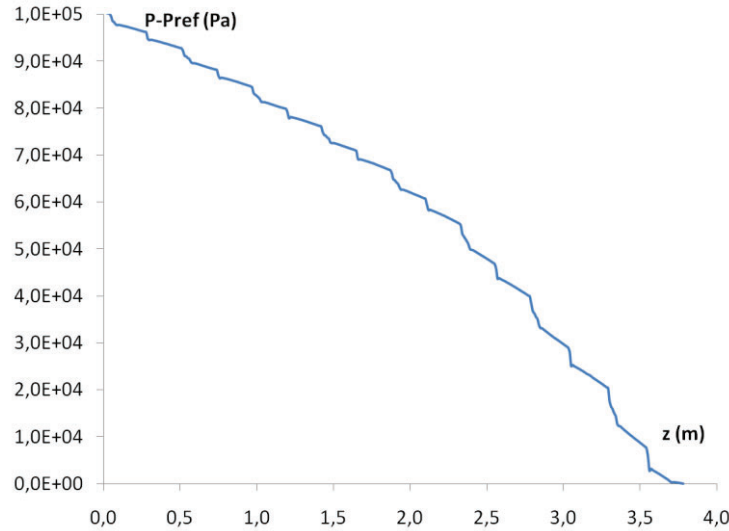


Figure 6. Mean pressure evolution against elevation for central sub-channel.

2. Turbulent intensity

One defines the turbulence intensity as the mean value (integral) of $I = \sqrt{\frac{2}{3}k} / U_{bulk}$ on a plane orthogonal to the main flow downstream of the mixing grid, k being the turbulent kinetic energy and U_{bulk} the bulk velocity. Available literature in the present field (see for example [28]) shows that the turbulent intensity downstream of a mixing grid varies between 15% and 30%.

Figure 7 gives the evolution of the mean turbulent intensity for the central sub-channel. The intensity of the turbulent kinetic energy has reasonable level and behavior (the decrease of the turbulent kinetic energy should be independent of the design of the mixing grid). Slightly more energy is resolved while the dimples and springs are represented and the evolutions in both simulations are similar.

Figure 7 shows the evolution of the fluctuations of each velocity component downstream the mixing grid

(for the component u , one has $I = \sqrt{\langle u'^2 \rangle} / U_{bulk}$, where u' is the fluctuation of the velocity component in the x direction, and $\langle \cdot \rangle$ stands for the time averaging operator). The intensity I_v of the other transverse component (v) is similar due to the central symmetry (the spatial integration is done over the central sub-channel). The level of the stream-wise and span-wise turbulent intensities are of the same order right after the exit of the mixing grid but the stream-wise velocity component becomes higher far downstream as the near-wall gradient is the only term that produces turbulent energy; a fully developed regime would be obtained if the bundle was long enough. The energy transfers between the different components are very complex and the corresponding analysis is not the aim of the present paper.

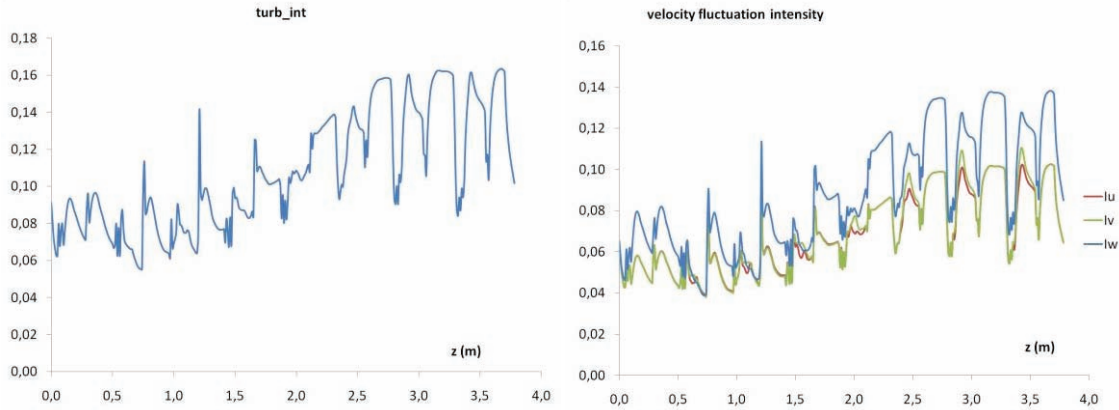


Figure 7. Mean turbulent intensity averaged over central sub-channel across the 7 MV and 8 SP.

3. Mean volume fraction, mean diameter and velocity field

The mean volume fraction for four central sub-channels is measured at three elevations. Table 5 gives a comparison between experimental and numerical results for the three points. We indicate the approximate minimum and maximum values computed by component and system codes of the PSBT benchmark. The simulated void fraction is overestimated by the current simulation at the lower and middle planes, and is closer to the experimental measurement at the upper plane.

Table 5 Mean void fraction for the four central sub-channel.

location	experimental	PSBT benchmark minimum	PSBT benchmark maximum	NEPTUNE_CFD
Lower (2216 mm)	0.46%	0.4%	5.5%	8.89%
Middle (2669 mm)	13.66%	7%	16%	21.84%
Upper (3177 mm)	37.84%	25%	34%	36.38%

Figure 8 represents the evolution of the mean bubble diameter averaged over the central sub-channel as a function of elevation. Whereas the mean bubble size increases with height, the influence of the simple spacers and mixing vanes on this variable can be noticed. The mixing grid has a greater effect than the simple spacer, but this one latter has still a significant effect. The mean diameter varies between 10^{-4} and 9.10^{-4} m with a maximum diameter of 1.6 mm in the middle of sub-channel where vertices are located (Figure 9). Coalescence is favored in these areas.

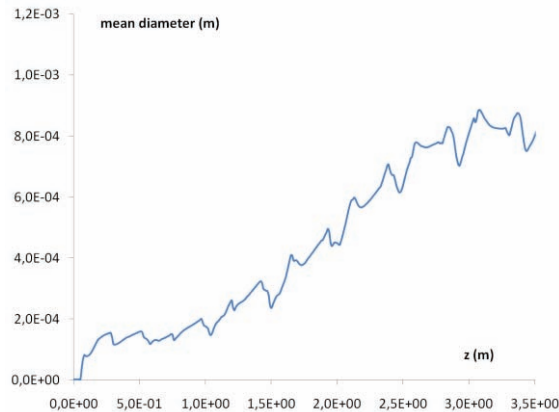


Figure 8. Mean diameter for central sub-channel.

Figure 9 shows the evolution of the mean tangential velocity at three distances from the end of the mixing vane, at respectively Dh , $3Dh$ and $5Dh$. The swirling flow generated by the vanes appears clearly, which is coherent with the existing literature; these ellipsoidal structures are observed experimentally by Chang et al. [28] for example. These cross-flows decrease when z increases. The velocity field seems to be more disturbed after the mixing grid. Strong exchanges between sub-channels are observed in particular close to the mixing grid.

Downstream the mixing grid, the shape of the swirl is ellipsoidal at the beginning; the main axis of this ellipse turns depending on the position of the plane and becomes circular at some distance, as the flow goes towards a homogeneous state in the transverse directions. Above the simple spacer, the behavior seems slightly different as secondary motions are observed.

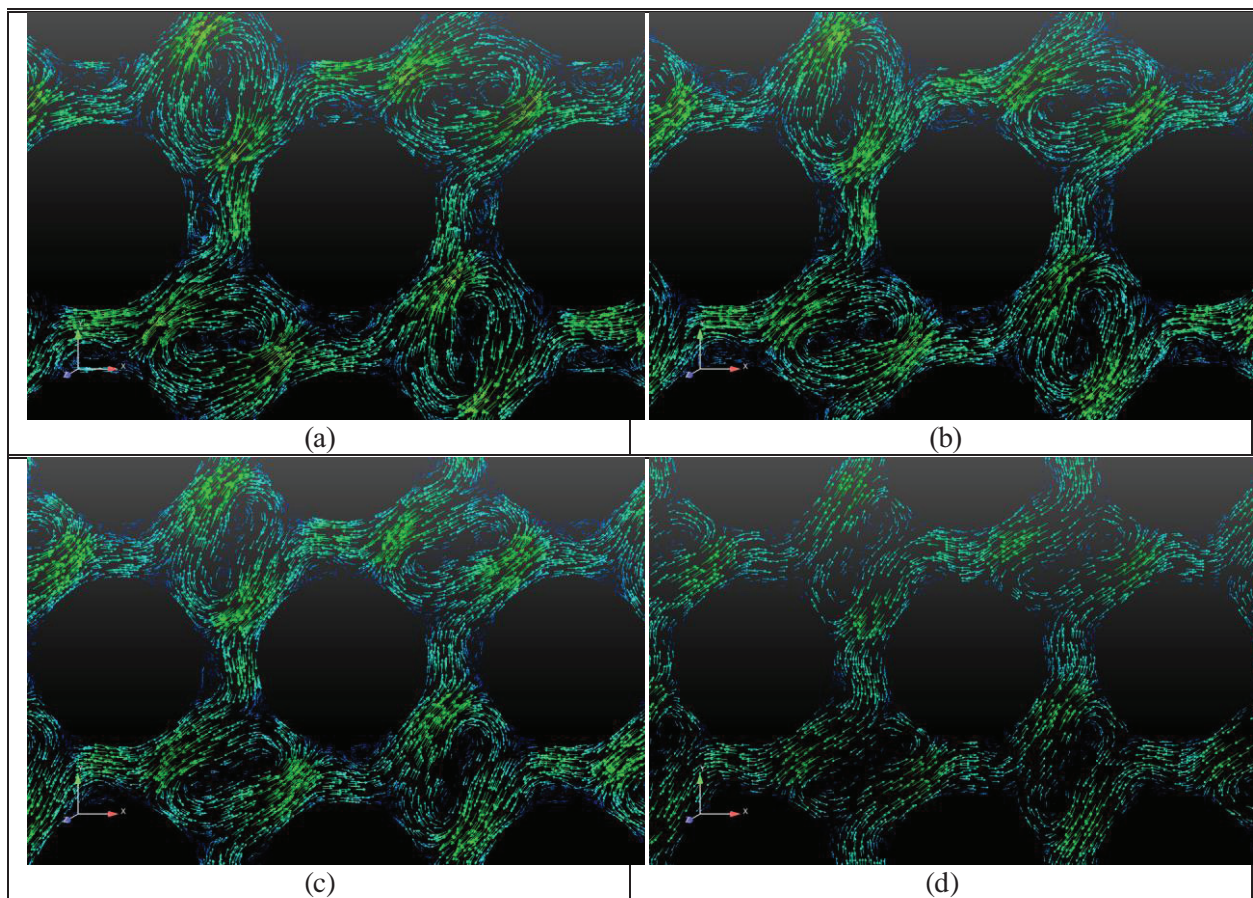


Figure 9. Tangential velocity at Dh (a), $3Dh$ (b), $5Dh$ (c), $8Dh$ (d) after the mixing vane.

Figure 10 shows the mean stream-wise velocity component at different distances from the mixing grid and the simple spacer. A deficit of the velocity is observed in the core of the swirals, that is usually observed in the presence of swirals but the values remain positive. The influence of the dimples and springs is clearly visible close to the mixing grid ($z = Dh$). The core of the vortex which may be observed with the velocity deficit is somewhat influenced by the obstacles (plane $z=3 Dh$). At $5 Dh$, a relative homogeneous velocity distribution can be observed. Velocities after the simple spacer are higher than after MV, especially in the core the sub channel and this effect is observed from Dh to $8 Dh$ distance from the obstacle.

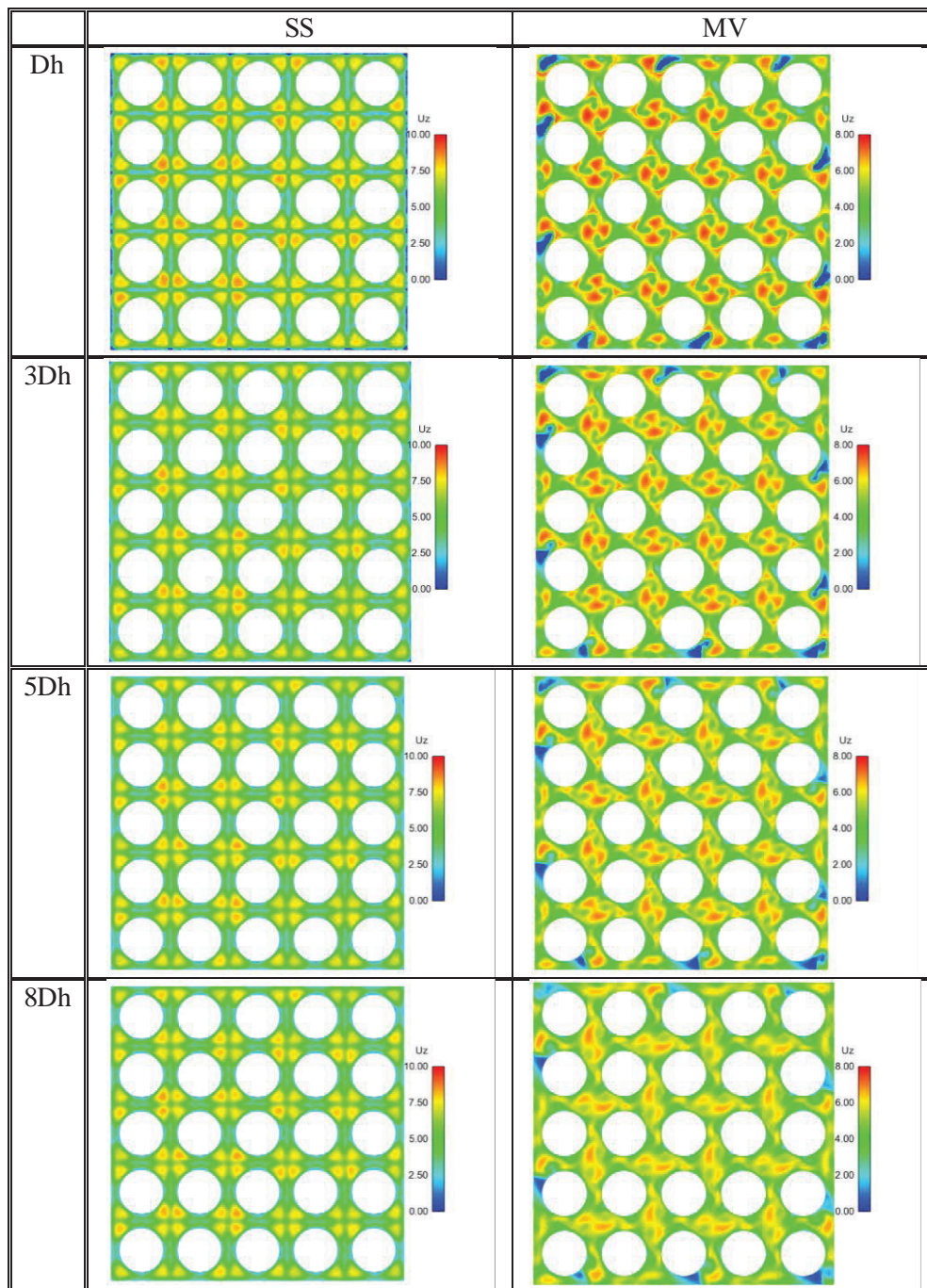


Figure 10. Stream-wise velocity component at Dh, 3Dh, 5Dh, 8Dh after the last mixing vane.

5. CONCLUSIONS

In the current paper, we presented a CFD simulation of the boiling flow taking place in the PSBT 5x5 fuel assembly with an official release version of NEPTUNE_CFD 2.3 and a standard set of models of the code for boiling flows. To the authors' knowledge, this work is the first industrial simulation of this kind on such a large mesh. We obtained a large number of information with this calculation and consequently, one of the first challenges was to sort and highlight actionable information. The computations over-estimate the

pressure drop but the mean void fraction is in good agreement with the experimental data given at three levels. We observed secondary flows and redistributions between sub-channels.

In further calculations, we will try to increase the heat flux to determine the departure from nucleate boiling (DNB) which has been measured in PSBT benchmark.

ACKNOWLEDGMENTS

This work has been achieved in the framework of the NEPTUNE project, financially supported by EDF (Electricité de France), CEA (Commissariat à l’Energie Atomique et aux Energies Alternatives), IRSN (Institut de Radioprotection et de Sûreté Nucléaire) and AREVA-NP.

The authors also thank OCDE/NEA, JNES and METI for having provided the detailed blueprints of the PSBT bundle.

REFERENCES

1. A. Douce, S. Mimouni, M. Guingo, C. Morel, J. Laviéville, C. Baudry, “Validation of NEPTUNE_CFD 1.0.8 for ADIABATIC BUBBLY FLOW AND BOILING FLOW”, Proceedings of CFD4NRS -3 Washington, USA, (2010)
2. A. Rubin, A. Schoedel, M. Avramova, “OECD/NRC benchmark based on NUPEC PWR subchannel and bundle tests”, volume 1 : experimental database and final problem specifications, NEA/NSC/DOC(2010)1
3. M. Ishii, N. Zuber, “Drag coefficient and relative velocity in bubbly, droplet or particulate flows”, *AIChE Journal*, Vol. **25**, No. 5, pp. 843-855 (1979)
4. N. Zuber, “On the dispersed two-phase flow in the laminar flow regime”. *Chemical Engineering Science*, Vol. **19**, p. 897 (1964)
5. A. Tomiyama, H. Tamai, I. Zun, S. Hosokawa, “Transverse migration of single bubbles in simple shear flows”, *Chemical Engineering Science*, Vol **57**, Iss. 11, pp.1849-1858 (2002)
6. B.S. Shin, S.H. Chang, “Experimental study on the effect of angles and positions of mixing vanes on CHF in a 2x2 rod bundle with working fluid R-134a”, *Nuclear Engineering and Design* **235** pp 1749-1759 (2005).
7. K. Ikeda, Y. Makino, M. Hoshi, “Single-phase CFD applicability for estimating fluid hot-spot locations in a 5x5 fuel rod bundle”, *Nuclear Engineering and Design* **236** (2006) 1149-1154.
8. W.K. In, T-H. Chun, C-H. Shin, “Numerical computation of heat transfer enhancement of a PWR rod bundle with mixing vane spacers”, *Nuclear Technology* vol. **161** JAN. 2008.
9. C.M. Lee, Y.D. Choi, “Comparison of thermo-hydraulic performances of large scale vortex flow (LSVF) and small scale vortex flow (SSVF) mixing vanes in 17x17 nuclear rod bundle”, *Nuclear Engineering and Design* **237** (2007) 2322-2331
10. C.C. Liu, Y.M. Ferng, C.K. Shih, “CFD evaluation of turbulence models for flow simulation of the fuel rod bundle with a spacer assembly”, *Applied Thermal Engineering* **40**, 389-396, (2012)
11. E. Krepper, B. Koncar, Y. Egorov, “CFD modelling of subcooled boiling – Concept, validation and application to fuel assembly design”, *Nuclear Engineering and Design* **237** 716-731 (2007).
12. A. Guelfi, D. Bestion, M. Boucker, P. Boudier, P. Fillion, M. Grandotto, J.-M. Hérard, E. Hervieu, P. Péturaud, “NEPTUNE – A new software platform for advanced nuclear thermal hydraulics”, *Nucl. Sci. Eng.*, Vol. **156**, pp. 281-324 (2007)
13. S. Mimouni, F. Archambeau, M. Boucker, J. Laviéville, C. Morel, “A second order turbulence model based on a Reynolds stress approach for two-phase boiling flow. Part 1: adiabatic cases ”, *Science and Technology For Nuclear Installations*, volume 2009, article ID 792395 (2009)

14. S. Mimouni, F. Archambeau, M. Boucker, J. Laviéville, C. Morel, “A second order turbulence model based on a Reynolds stress approach for two-phase boiling flow. Part 1: Application to the ASU-annular channel case”. *Nuclear Engineering and Design* **240**, Iss. 9, pp. 2233-2243 (2010)
15. Falk, F., Giacomelli, A., 2003. Rapport d’essais AGATE PROMOTEUR DE MELANGE”, technical report CEA DTP/SETEX/LTAC/03-191. Internal Report in French.
16. Archambeau F., Mechtoua N, Sakiz M., “A finite volume code for computation of turbulent incompressible flows – industrial applications”. *International Journal on Finite Volumes* volume 1 (2004)
17. Falk, F., Hugonnard, R., 2002. Rapport d’essais DEBORA PROMOTEUR DE MELANGE, essais de BO et de topologie, campagne 4800-4900-5000”, Technical Report, CEA DTP/SETEX/LTAC/02-158. Internal report in French.
18. M. Ishii, “Thermo-fluid dynamic, theory of two-phase”, Eyrolles (1975)
19. N. Mechtoua., M. Boucker., J. Laviéville, J.-M. Hérard, S. Pigny, G. Serre, “An unstructured finite volume solver for two phase water/vapour flows based on an elliptic oriented fractional step method”. Proceedings of the 10th Int. Topl. Mtg. Nuclear Reactor Thermal Hydraulics (NURETH 10), Seoul, Republic of Korea, (2003)
20. SALOME: web site : <http://www.salome-platform.org>
21. M. Lance, M. Lopez de Bertodano, “Phase distribution phenomena and wall effects in bubbly two-phase flows”. In: Hewitt, G.F., Kim, J.H., Lahey Jr., R.T., Delhay, J.M., Zuber, N. (Eds.), *Multiphase Science and Technology*, Vol. 8. Begell House, pp. 69–123. (1994)
22. N. Kurul, M. Podowski, “Multidimensional Effects in Forced Convection Subcooled Boiling,” Proceedings of the 9th International Heat Transfer Conference, Jerusalem, Israel, Vol. 1, p. 21 (1990)
23. H.C. Unal, “Void fraction and incipient point of boiling during the subcooled nucleate flow boiling of water”, *International Journal of Heat and Mass Transfer* 20, 409-419 (1977)
24. S. Mimouni, F. Archambeau, M. Boucker, J. Laviéville, and C. Morel, “A Second-Order Turbulence Model Based on a Reynolds Stress Approach for Two-Phase Flow. Part I: Adiabatic Cases”, *Science and Technology of Nuclear Installations*, Vol 2009, Article ID (2008)
25. P. Ruyer, N. Seiler, M. Beyer, F.P. Weiss, “A bubble size distribution model for the numerical simulation of bubbly flows”, Sixth International Conference on Multiphase Flows, ICMF2007, Leipzig, Germany (2007)
26. Best Practice Guidelines for the use of CFD in Nuclear Reactor Safety Applications, NEA/CSNI/R(2014) 11
27. J. Laviéville, “Un algorithme stationnaire pour Neptune_CFD”, technical report, H-I81-2014-12169-FR, available upon request (2014)
28. S.K. Chang, S. K. Moon, W. P. Baek and Y. D. Choi, “Phenomenological investigations on the turbulent flow structures in a rod bundle array with mixing devices”, *Nuclear Engineering and Design*, 238, pp.600–609 (2008).